G. Di Martino, A. Iodice, D. Riccio, G. Ruello, and I. Zinno, "Angle Independence Properties of Fractal Dimension Maps Estimated from SAR Data," *IEEE J. Sel. Topics Appl. Earth Observ.*, vol. 6, no. 3, pp. 1242-1253, June 2013. DOI: 10.1109/JSTARS.2013.2248134.

Angle Independence Properties of Fractal Dimension Maps Estimated from SAR Data

Gerardo Di Martino, *Member, IEEE,* Antonio Iodice, *Senior Member, IEEE,*
Daniele Riccio, *Senior Member, IEEE,* Giuseppe Ruello, *Member, IEEE,* and Ivana Zinno

***Abstract* — The extremely remarkable properties of angle independence exhibited by an innovative SAR product, the fractal dimension map estimated from a single SAR image, are discussed. The theoretical analysis is supported by a noticeable data set of actual SAR images acquired, with look angles varying from 20° to 45°, in the stripmap operational mode by the COSMO-SkyMed constellation. The behavior of the fractal dimension maps at different look angles is discussed for both natural and urban scenarios and emphasis is also posed on areas within the same image that, according to the scene macroscopic topography, are characterized by different incidence angles. The whole analysis is aimed at highlighting, on the one hand, the specific independencies of natural surface fractal dimension maps from the look angle and from the local incidence angle, which can be very useful in information extraction and SAR post-processing techniques and, on the other hand, the different fractal dimension maps behavior whereas urban areas are analyzed.**

***Index Terms*— Synthetic Aperture Radar, Rough Surfaces, Fractals, Electromagnetic Scattering.**

I. Introduction

Developing tools for SAR data interpretation and information extraction is a key issue within the remote sensing community [1]. In fact, SAR products end users are mostly interested in monitoring physical parameters characterized by a clear and precise meaning within their scientific arena, and generally prefer data provided in easy-to-use formats. Within this respect the standard SAR images are not significantly appealing since they provide in a typical SAR coordinate system (e.g., azimuth-slant range) quantitative information on a typical SAR entity (the scene radar reflectivity). Even if (actually not straightforward) geocoding algorithms are implemented, the obtained images are certainly not easy to use in practical applications since they still remarkably depend on SAR sensor parameters and acquisition geometry, and are linked in a very involved way to (too) many scene parameters holding a clear physical meaning. Therefore, use of SAR images is severely limited to radar sensor experts since it requires supervised analysis to support any major image application. Hence, to be fruitful, SAR data interpretation and information extraction tools should allow obtaining reliable value-added products able to provide meaningful information

G. Di Martino, A. Iodice, D. Riccio, and G. Ruello are with the Dipartimento di Ingegneria Elettrica e delle Tecnologie dell'Informazione, Università di Napoli Federico II, 80125, Napoli, Italy (e-mail: gerardo.dimartino@unina.it; iodice@unina.it; daniele.riccio@unina.it; ruello@unina.it).

I. Zinno is with Istituto per il Rilevamento Elettromagnetico dell'Ambiente, Consiglio Nazionale delle Ricerche, 80127 Napoli, Italy (e-mail: zinno.i@irea.cnr.it).

regarding the imaged scenes, hopefully directly provided in a reference system independent of the SAR sensor.

Whenever the focus is on the analysis of natural surfaces, fractal models provide the better way to deal with this class of problems [2]-[13] and identify the physical quantities of interest in the applications. As a matter of fact, the use of fractal dimension is widespread within many scientific communities such as geologists [6]-[12], astronomers [9], [14], [15], engineers [3], [16], [17], oceanographers [18], [19], and, more in general, mathematicians and physicists [2]-[5]. Fractals are widely used by geologists to correctly model the behavior of a wide set of natural phenomena - such as the roughness of natural surfaces [6]-[10], the characterization of different types of lava flows [11]-[12], the topography of solar system planets and of their natural satellites [9], [14] - and to characterize the geomorphology and geodynamics of natural surfaces [6]; within this framework, the fractal dimension is a concise and meaningful entity with solid mathematical and physical background that bears crucial information for the geometrical and, much more interestingly, also for the geophysical characterization of the surface [6]-[14]. More specifically, the fractal dimension is normally used by geologists to model the roughness of natural surfaces being, in theory and in practical measurements, not dependent on the size of the observed surface, thus solving problems typical of classical statistical roughness descriptors, such as the height standard deviation and correlation length, that depend on both the scale and the size of the area on which they are estimated [6]-[10].

Once the meaningful physical entity to be estimated is identified (e.g., the fractal dimension), theory to retrieve it from the standard SAR images must be provided. In [20] and [21] some of the authors introduced new models for the imaging of natural surfaces and discussed results regarding the estimation of the fractal dimension directly from a SAR image. The proposed approach is applicable to local areas within the SAR image thus allowing generation, as output, of a new "image", the *fractal dimension map*, i.e., a point by point map of the estimated fractal dimension of the imaged surface. In [22] and [23] the proposed algorithm was applied on actual SAR high resolution data and the first examples of fractal dimension maps were presented. Hence, the result of our elaboration is not a single value for each considered SAR image, but a map accounting for local variations of the surface fractal dimension. Such a map can be geocoded via standard techniques and then used in conjunction with other providers of physical information, e.g. geological maps. Some properties of the technique we propose are remarkable. First of all, the whole elaboration is fully based on reliable and reproducible mathematical models (no heuristic or empirical models are employed) thus being potential object of improvements and further physical interpretations [24]. In addition, by estimating the fractal dimension, we are able to provide a local roughness parameter by means of a single image (neither interferometry approaches nor other techniques based on phase difference SAR images are required). Moreover, we estimate the local fractal dimension of a surface which bears a very precise physical meaning and is used by a wide range of scientific communities: this sound as a very important property because, other kinds of meta-parameters, frequently used for information extraction from SAR data, have a meaning that is accessible to SAR experts only. With this respect, a more general comment on

SAR products and their use is then in order. One of the main challenges in SAR data interpretation is due to the presence of a huge amount of information within each image: the list of the parameters influencing SAR image formation is very long [3], [19]. In fact, both scene and sensor parameters affect the formation of a SAR image: just to list the main ones, among the scene parameters (that are local entities, i.e., depend on the considered pixel of the SAR image) we must mention the surface complex dielectric constant and the surface roughness (here described in terms of fractal parameters) that also introduces a dependence on the local incidence angle; among sensor electronic parameters we list the polarizations of the transmitted and received signals, the SAR chirp carrier frequency and bandwidth, the sampling rate (Pulse Repetition Frequency), the antenna dimensions, these parameters determining also SAR resolutions and coverage; finally, among SAR sensor orbital data we list the sensor height and velocity and the look angle. Thus, the inherent complexity of information extraction from SAR images is strictly related to the problem of somehow separating on some SAR product (hopefully, isolating, so to generate a specific "new" image) the effects of the parameter of interest from other kinds of effects. As a matter of fact, the fractal dimension seems to excellently fit this last requirement, because it clearly depends on a single feature of the observed scene, namely its roughness, whose estimation opens the way to a wide range of practical applications in view of its clear physical meaning. We underline that this nice dependence property is definitely uncommon among other entities estimated from the available SAR products. As a matter of fact, in many practical situations the post-processing of SAR images provides entities showing a significant dependence on the acquisition geometry of the employed SAR image. This is a major disadvantage from the end users viewpoint. For instance, the severe dependence on the SAR acquisition geometry lead to classification maps that cannot be easily compared by the non SAR sensor expert if obtained from SAR images acquired from different satellite tracks. Similarly, the severe dependence on the local incidence angle leads to estimate soil moisture maps that can significantly change over areas that are homogeneous according to the soil water content, but differing in topography [25]. These examples provide intuitive severe limitations to corresponding application purposes.

For the above reported reasons, in the present paper we investigate value-added properties of the fractal dimension maps and, in particular, we study potential dependencies on the SAR look angle and the local incidence angle. Indeed, products which are independent of these parameters provide many advantages and greatly simplify the adoption of SAR data from the different end users communities. As a matter of fact, look angle independence allows continuous monitoring through the joint use of data coming from different data sets relevant to the same area, independently of the acquisition track. Moreover, incidence angle independence provides the possibility to an almost continuous monitoring obtained by joining almost any SAR image on a certain area irrespective of the different acquisition geometries. In fact, in this case the product does not depend on the shading: incidentally, we note that this property could be potentially used in support of shape-from-shading techniques, in order to someway remove the dominating shading effect and its relation with the surface topography [26], [27]. Finally, a product

showing this kind of sensor independencies is very useful in support of data fusion schemes, since it provides fundamental input data for the use of physical-based models in SAR segmentation and classification [28].

In this paper the fractal dimension maps generated by this innovative SAR image processing applied to a set of actual SAR images acquired by the same sensor and relevant to the same area, but with different look angles, are analyzed and compared for the first time. For the analysis we employ a set of COSMO-SkyMed stripmap SAR images relevant to the area of Naples, Italy, and its surroundings, thus including both urban areas and natural ones (the Somma-Vesuvius volcanic complex): resolution is in any case 3x3 m^2, while the SAR look-angle varies from 20° to 45° in the different images, whereas the local incidence angle significantly changes within the same image for the specific macroscopic topography of the volcanic area. The fractal dimension map is estimated all over each SAR image, irrespective of whether natural or manmade features are present. As a matter of fact, natural and man-made areas are expected to present a very different behavior when fractal dimension estimation is performed. By hypothesis our model is expected to perform correctly (or at least "well") on natural areas, whose behavior fall within our theoretical model assumptions. In this case the retrieved values of the fractal dimension are expected to fit well with the expected ones. Conversely, in case of application on man-made areas the algorithm provides values which cannot be assumed as the fractal dimension of the imaged area. The study of the properties held by fractal dimension maps estimated on man-made areas is of key importance from the viewpoint of the present work, because not-always these areas can be masked out from the images (in particular, when dealing with isolated buildings), thus implying that a study of their behavior is a prerequisite for the interpretation of fractal dimension maps. Furthermore, the values provided by our algorithm on man-made zones, though not bearing a precise physical meaning, could provide a valuable support for the identification of urban areas [29].

The paper is organized as follows. In Section II the theoretical background of our imaging model is summarized, with particular attention to potential dependencies on the sensor parameters of interest. In Section III the experimental setup and the available data set are described in detail. Relevant comments on the obtained results are reported in Section IV. Finally, Section V bears the concluding remarks.

II. IMAGING MODEL

In the present section we summarize the main theoretical and implementation aspects regarding the generation of the fractal dimension map from a single SAR image relevant to a natural surface. In the last decades many studies highlighted the weaknesses of classical surface stochastic models when used for the description of natural scenes [2]-[10], and demonstrated that this class of surfaces can be effectively modeled by means of fractal geometry [2]-[5]. Following these guidelines, we here consider the fractional Brownian motion (fBm) model, which is an everywhere continuous, nowhere differentiable process, and

can be conveniently described in terms of its increment probability density function (pdf) [3]-[5]. In particular, a stochastic process $z(x,y)$ is an (isotropic) fBm surface if, for every x, x', y, y' it satisfies the following relation:

$$\Pr\{z(x,y) - z(x',y') < \bar{\xi}\} = \frac{1}{\sqrt{2\pi}s\tau^H} \int_{-\infty}^{\bar{\xi}} \exp\left(-\frac{\xi^2}{2s^2\tau^{2H}}\right) d\xi, \quad (1)$$

where τ is the distance between the points (x,y) and (x',y'); H and s are the two parameters here selected to control the fBm behavior in the spatial domain, and are respectively defined as:

- H: the *Hurst coefficient* ($0<H<1$), related to the fractal dimension D through the relationship $D=3-H$;
- s [m^{1-H}]: the *incremental standard deviation*, i.e., the standard deviation of the surface increments at unitary distance.

It has been demonstrated that the Power Spectral Density (PSD) of the isotropic two-dimensional fBm process exhibits an appropriate power-law behavior [2]-[5]:

$$S(k) = S_0 k^{-\alpha}, \quad (2)$$

wherein S_0 and α are the fBm spectral parameters, related to the spatial ones by the following relationships [3]:

$$S_0 = 2^{H+1}\Gamma^2(1+H)\sin(\pi H)s^2 \quad (3)$$

$$\alpha = 2 + 2H = 8 - 2D, \quad (4)$$

$\Gamma(\cdot)$ being the Euler Gamma function.

In [21] some of the authors presented a forward model linking the stochastic characterization of a SAR image to the fractal parameters of the observed surface. In the same work also an algorithm for the estimation of the fractal dimension of natural surfaces from their SAR images was introduced. In the present paper an analysis of the behavior of the algorithm for changing illumination conditions is performed. In order to provide a better insight into the experimental framework presented in the following sections, hereafter we summarize the main theoretical aspects of the imaging model on the grounds of which the estimation algorithm has been developed.

We start with the assumption that between the SAR image $i(\cdot)$ and the reflectivity function of the scene a linear relation involving the impulse response of the sensor can be invoked [21]:

$$i(x',y') = \iint \gamma(x,y)\mathrm{sinc}\left[\frac{\pi}{\Delta x}(x'-x)\right]\mathrm{sinc}\left[\frac{\pi}{\Delta y\, sin^2\,\theta_0}(y'-y)\right]dxdy, \quad (5)$$

where x and y, as well as x' and y', represent azimuth and ground-range, respectively; $\gamma(x,y)$ is the two-dimensional reflectivity pattern of the scene; θ_0 is the look angle of the sensor, and Δx and Δy are the azimuth and ground-range SAR geometric resolutions, respectively. Note that (5) is the ground range counterpart of the original slant range equation, where a simple conversion to ground range geometry has been performed [21].

The geometrical features and the physical properties of the observed surface affect the formation of the final SAR image through the reflectivity function. From (5) it can be stated that the autocorrelation of the image is the convolution between the autocorrelation of the reflectivity function and the autocorrelation of the sinc functions, which implies a band-limiting effect (linked to the SAR resolution) on the image spectrum, with respect to the reflectivity one [21]. Hence, in order to retrieve the information of interest, a model of the reflectivity function must be introduced. The authors demonstrated that - in the hypothesis of a small slope regime for the surface roughness - the modulus of the reflectivity function $|\gamma(x,y)|$ - which is in fact simply related to the normalized radar cross section σ° - depends, to the first order, on the partial derivative $p(x,y)$ of the surface height in the range direction. Hence, in a first order approximation no dependence on the partial derivative of surface height in the azimuth direction $q(x,y)$ is present [21]:

$$|\gamma(x,y)| = \sqrt{\sigma^\circ(p,q)} = a_0 + a_1 p(x,y) + o(p,q), \quad (6)$$

where a_0 and a_1 are the coefficients of the Mc Laurin series expansion, depending on the specific scattering model that is considered, and $o(\cdot)$ stands for small O notation. We explicitly note that the small slope assumption holds in a very wide range of practical situations, because natural surfaces presenting slopes larger than 20% are not so common. The coefficients a_0 and a_1, and in turn the validity limits of the proposed model, depend on the considered look-angle, the fractal parameters of the observed surface, and the scattering model. As an example, in [21] the coefficient a_1 is analytically evaluated in closed form whenever the Small Perturbation scattering fractal Model (SPM) [3] is employed as:

$$a_1 = \sqrt{A_0} cos\theta_0\, sen^{-H}\theta_0[2 + (1+H)cos^2\theta_0\, sen^{-2}\theta_0], \quad (7)$$

where $A_0 = \frac{S_0 \kappa^{1-2H} |\beta_{mn}|^2}{2^{2H}}$, κ is the electromagnetic wavenumber and β_{mn} is a polarizations dependent factor [3]. Whenever a different scattering model is assumed, the expression in (7) changes (equation (6) do not), but nonetheless it will show dependencies on the same quantities and in particular on θ_0.

In [21] a closed form expression for the PSD of azimuth and range cuts of the derivative process $p(x,y)$ has been evaluated via appropriate Fourier transforms of their autocorrelation. The noticeable expression of the range cut PSD is

$$S_p(k_y;\Delta y) = 2s^2 \Delta y^{-1+2H} \Gamma(1+2H) \sin(\pi H)\left[1-\cos\left(|k_y|\Delta y\right)\right] \frac{1}{\left(|k_y|\Delta y\right)^{1+2H}}, \quad (8)$$

where k_y is the spatial wavenumber associated to the range direction and Δy is the ground range resolution of the image [20], [21]. Moreover, it has been demonstrated that for small wavenumbers the range cut PSD holds a linear behavior in a log-log plane, while the azimuth cut PSD does not present this remarkable property [21]. In particular, when $k_y \Delta y \to 0$ we obtain the following asymptotic expression for the range cut PSD, $\tilde{S}_p(k_y)$:

$$\tilde{S}_p(k_y) = s^2 \Gamma(1+2H) \sin(\pi H) \frac{1}{|k_y|^{2H-1}}. \quad (9)$$

From (5) we obtained that the PSD S_i of the SAR image can be evaluated as the convolution between the autocorrelation of the reflectivity function and the autocorrelation of the sinc functions. Hence, taking into account the relation between the reflectivity and the derivative process p reported in (6) we obtain for S_i the following expression:

$$S_i(k_y) = a_1^2 S_p(k_y;\Delta y) \mathrm{rect}\left[\frac{\Delta y \sin^2 \vartheta_0 \, k_y}{\pi}\right], \quad (10)$$

where, in a significant range of small wavenumbers, the asymptotic expression in (9) can be assumed for S_p**.** To provide a graphical counterpart of these considerations, in Fig. 1 the azimuth (dash-dot line) and range (continuous line) PSD of an image are shown in a log(k) - log(|S(k)|) plane. In this example we assumed s=0.1 m^{1-H}, H=0.7 and a_1=1; as a reference, also the behavior of the PSD of a cut of the fBm surface with the same fractal parameters (dashed line) is reported. Note that in the figure the wavenumbers are normalized to the value of the considered resolution. Figure 1 allows appreciating the linear behavior of the graph of the range cut PSD, asymptotically assumed for small wavenumbers.

As a matter of fact, the asymptotic spectrum reported in (9) shows the meaningful property of exhibiting a linear behavior in a log-log plane: in particular, looking at the power-law exponent in (9) we conclude that the line slope is equal to $1-2H$. Therefore, the joint use of (9) and (10) allows the implementation of linear regression techniques for the retrieval of the fractal parameters of an observed scene directly from its corresponding SAR image. In order to exploit this remarkable property, an algorithm has been developed allowing the retrieval of the point by point fractal dimension map of a natural surface starting from its single look amplitude SAR image [21], [22]. The algorithm evaluates the fractal dimension D associated to each pixel using the information relevant to neighboring pixels enclosed in a sliding window which, spanning the whole image, generates the fractal dimension map. Note that the estimation of the PSD of range cuts enclosed in the window is performed by using the Capon estimator [21], [24]. Then a linear regression step on the obtained PSD allows the evaluation of the fractal dimension D. The Capon estimator was originally proposed for the analysis of geospatial data in presence of a very limited number of samples and customizes a filter centered at each frequency of interest which minimizes the power output subject to the constraint that the central frequency gain is unitary [30], [31]. Therefore, the filter minimizes out-of-band power and has been chosen to overcome the leakage and high variance problems which rise when facing the estimation of power law spectra, as detailed in [13], [30] and [31].

One of the main goals of this work is to explore the influence of the look angle on the estimation of the fractal dimension map. Looking at (7), (9) and (10) it can be noted that the image PSD S_i depends on the look angle θ_0 only through a_1. At the same time, we note that the fractal dimension estimated using the proposed technique depends only on the spectral exponent, which in turn does not depend on a_1 being equal to $1-2H$. Therefore, the estimation result is expected to be independent of the sensor look angle, at least if the validity of the model in (6) for the considered sensor and surface parameters is assumed. For the same reasons, the estimated fractal dimension is expected to be independent of the local incidence angle and, equivalently, of the absolute value of the surface derivative process. This fact supports the idea that fractal dimension estimation performed on areas which can be considered homogeneous from the viewpoint of the roughness at resolution scale, but which present also very different macroscopic slopes (e.g., the case of the fore and back-slope regions of a mountain), should provide the same estimates.

The presented theoretical conclusions are obtained under at least two assumptions: the linear approximation which leads to (6) and the asymptotic evaluation which brings to the expression in (9). Therefore, when working with actual SAR images, two different issues can arise: on one side, the validity of the model in (6) cannot be always safely assumed; on the other side, non linear effects can appear w.r.t. spectral components where the full model in (8) should be considered in place of the asymptotic one in (9). In the following sections we investigate the dependency of the fractal dimension estimation results on the SAR viewing angle through a comprehensive experimental framework, and we highlight the different behavior of natural and man-made areas – i.e., areas where the model is expected not to hold.

III. Experimental Framework

In order to perform the experimental fractal analysis object of the paper, a set of COSMO-SkyMed images has been considered. The data set is made up of three HH-polarized stripmap SCS_U (Single-look Complex Slant Unbalanced) images relevant to the area of Naples and its surroundings. Images have been acquired in ascending orbit with look angles of 22°, 31° and 44°, on 3 September 2011, 1 August 2011 and 3 August 2011, respectively. The resolution of each considered image is 3x3 m^2 in azimuth-ground range geometry. The considered data set being made up of stripmap SCS_U images represents the most "conservative" available Cosmo-SkyMed product. On this kind of data no radiometric equalization is performed in terms of compensation of both range antenna pattern and incidence angle; only compensation of the antenna transmitter gain and receiver attenuation, as well as range spreading loss is applied. In addition an un-weighted SAR processing is performed, i.e. no windowing is applied on the processed bandwidth. Therefore, no full internal calibration is applied on these images. The choice fell on this kind of data in order to avoid any possible source of distortion of the fractal features present in the image, where this event is in general caused by "human" manipulation of the acquired SAR images [23]. However, we note that for the estimation of most of the geophysical entities that are estimable from SAR images, the calibration step is definitively required to avoid unacceptably reducing the attainable performances of the analysis: this marks a very strong limitation in corresponding SAR product usage [32], [33]. In the present paper, we compare the fractal dimension maps generated starting from different SAR acquisitions and in absence of a complete calibration step. The calibration independence shown here is another very remarkable characteristic, potentially allowing a wider use of the SAR product we propose.

From the considered SAR images two regions of interest have been selected and cropped, one relevant to the urban area surrounding the business district and the central station of Naples, and the other relevant to the mainly natural area of the Somma-Vesuvius volcanic complex. In order to obtain the fractal dimension maps relevant to these areas the algorithm described in the previous section has been applied. The cropped images together with the obtained fractal dimension maps for the two regions of interest are presented in Fig. 2, on the left and right column respectively. Relevant differences can be visually appreciated between the SAR images of the same areas acquired with the different look angles.

All the maps have been geocoded using a standard technique based on the SRTM DEM of the area of interest and have been interpolated in order to obtain a pixel spacing of 5x5 m^2. The geocoding step is necessary whenever the focus is on the comparison of data acquired with significantly different look angles; furthermore, the use of geocoded products is of fundamental importance for the applicative community (e.g., geologists, geophysicists), which frequently has little experience on SAR reference system issues, but is used to manage geo-referenced data. In particular, fractal dimension maps could be used in

conjunction with other kinds of physical information (e.g., geological maps, land use maps), which are usually provided in a cartographic geodetic reference system. However, the geocoding step cannot be applied on SAR images prior to the fractal dimension estimation step, since it completely degrades the fractal characteristics present in the image [23]: the sole available option is to perform the fractal estimation on non-geocoded images and then apply the geocoding directly on the fractal dimension maps. As a matter of fact, the geocoding procedure can induce significant radiometric artifacts on the maps, especially in areas where geometrical distortions due to the SAR acquisition geometry are severe. For the case of interest, this can be observed on the geocoded fractal dimension maps shown in Fig. 3, where the different impact of the geocoding step on the images at varying look angles can be appreciated. In particular, it can be noted that in the Somma-Vesuvius region the artifacts are more evident in the fractal dimension map relevant to the 22° look angle image, where a heavier interpolation was required. Anyway, in the natural areas, where the imaging model in (6) can be assumed to hold, no significant degradation of the estimates should be introduced by the geocoding procedure, since the geometrical distortions are very low in areas where the surface shows sufficiently small slopes. On the contrary, where the surface slope becomes considerable, as for the volcanic cone or the Somma mountain, giving rise to geometrical distortions represented in the SAR image by strong layover or shadowing effects, the fractal dimension estimation is not reliable both for the important degradation introduced by the geocoding and (mainly) for the lack of validity of the imaging model [23]. Due to the geometrical distortions present in SAR images, whose entity changes according to the look angle of the sensor, the mapping between the pixels present in the geocoded image and those on the original non-geocoded SAR image changes for different look angles. Indeed, the number of pixels representing a certain area on a SAR image depends on the acquisition geometry of the sensor and on the topography of the considered zone [33]. As a matter of fact, the behavior of the fractal dimension maps shows a greater sensitivity to different sensor look angles in the areas where the distortions due to topography are larger. Furthermore, we expect that the effects of geocoding can be significant in presence of man-made structures, where the main problem is the displacement of the image features related to strong scattering mechanisms due to the lack of adequate models accounting for the presence of the buildings and of their SAR image signatures [34], [35]. Looking at the images in Fig. 3 (d)-(f), we can note that artifacts are less evident than in the Somma-Vesuvius maps; nonetheless, in the urban case building features displacements - which can be hardly appreciated looking at the fractal dimension maps - can be more significant than interpolation artifacts.

In order to perform a comprehensive analysis, for each of the two regions of interest four different areas have been selected for testing. Concerning the SAR image relevant to the Vesuvius area, four cuts performed on diverse sides of the volcano have been considered: this analysis is devoted to investigate the behavior of the fractal dimension map in presence of different illumination conditions of the same structure. In particular, we can classify the selected patches with reference to the sensor acquisition characteristics which are common to the whole data set: ascending track, almost parallel to the geographic North and right

looking antenna. Taking as a reference this kind of acquisition geometry we define the image subsets as follows: the first one is relevant to the Vesuvius back-slope zone (East), the second one to its fore-slope (West), the third to the forward sensor direction (North) and, finally, the last one to the backward sensor direction (South). With regard to the SAR image of the urban area, the patches have been selected to represent different types of city scenarios: in particular, the first zone is relevant to a modern business district, the second one to a semi-urban area (i.e., characterized by a less dense building distribution), the third to a part of the city historical center and the last one to a sea area. The sites under test are all enclosed in a 200x200 pixel window, corresponding to a geographical area of 1x1 km^2, which is chosen as homogeneous as possible with respect to significant physical properties of the underlying scene (e.g., surface roughness, geophysical characteristics, presence of similar urban structures, and average height of the buildings). The different test sites are marked in red over the geocoded fractal dimension maps presented in Fig. 3.

IV. Results Discussion

In Tab. I and II we present the results of the statistical analysis of the considered natural and urban subsets, respectively. In Fig. 4 the histograms relevant to the eight different test sites are reported and those relevant to the different look angles are compared in each plot. This kind of statistical analysis, based on the study of the average behavior of the fractal dimension within a window, is fully justified by the fact that the proposed product is devoted to the applicative community, which is typically interested on geophysical characteristics of homogeneous areas, rather than on punctual characteristics related to the statistical behavior of single image pixels. Moreover, this type of analysis, based on the overall statistical behavior of the maps within a window rather than on the comparison of punctual values, should also limit the negative effects of geocoding, which were pointed out in the previous section.

With reference to the comparison of the obtained results, we are interested mainly in three criteria allowing to state that the fractal dimension maps are independent of the sensor look angles:

1) the mean variations are small with respect to the standard deviations;

2) the standard deviation variations are small;

3) no significant differences can be appreciated in the histograms, both w.r.t. the percentile values and by visual inspection.

Looking at the numerical results displayed in the tables, the difference between the behavior in the natural and in the urban case with respect to the above criteria is evident. In particular, for the natural area case the variations of the mean D_{mean} are significantly smaller than the standard deviations D_{stdev}, implying that the average fractal dimensions evaluated at different look angles and on different areas of the Vesuvius are practically indistinguishable. Moreover, in the natural areas the obtained values

of D_{stdev} are in the range [0.06, 0.08], i.e. almost equal for all the examined cases, and the histograms presented in Fig. 4 (a)-(d) and (h), apart from minor effects, show a very similar behavior. Furthermore, looking at the values of $D_{1\%}$ and $D_{99\%}$ reported in Tab. I - which account for the first and 99th percentile, respectively - it can be noted that they are all very similar and less than 1% of the pixels presents a value of the fractal dimension lower than 2.1 and less than 1% a value larger than 2.5 in all the reported cases: practically, the fractal dimension is enclosed in the range]2, 2.5[, i.e. in the typical range of natural surfaces [2]-[12]. Hence, fractal dimension maps of natural scenarios characterized by the same mean roughness can be considered to be independent of the sensor look angle and of the mean local incidence angle, also for very important variations of these quantities as in the considered case: 22°-44° look angles and opposite mountainsides of the volcano.

Conversely, concerning urban areas, the differences between the values of the fractal dimension means at different look angles are often of the order of D_{stdev} (see the case of 22° and 44° look angle images). Furthermore, in the urban areas the standard deviations are in the range [0.12, 0.18], i.e. nearly doubled with respect to those of natural surfaces - due to the unstable behavior of the technique when applied on zones where the underlying model does not hold [29] - and in many cases (business district above all) they experience larger differences with respect to natural areas. Finally, looking at the histograms in Fig. 4 (e)-(g) significant differences can be appreciated: in particular, looking also to the values of the percentiles reported in the Tab. II it can be noted that a significant part of the fractal dimension values fall out of the range]2, 2.5[, due to the non-fractal characteristics of the examined areas [29], and that the percentile values experience relevant variations for maps estimated at different look angles. For these reasons, we can state that the fractal dimension value estimated in urban areas can be considered to be dependent on the sensor look angle. It is worth noting, however, that all these different types of urban areas share a common behavior as the sensor look angles increases: D_{mean} values decrease and D_{stdev} values increase, i.e. the histograms of the fractal dimension maps of the urban zones tend to translate toward lower values of the fractal dimension and to widen out for increasing look angles. Moreover, some difference between the different types of urban areas can be appreciated in the distribution tails: in fact, for the business district the values of $D_{99\%}$ in Tab. II are slightly higher. Finally, we explicitly note that the fourth zone of Tab. II - which is the one relevant to the sea - follows the behavior outlined for natural surfaces and its statistics are very similar to those reported in Tab. I, except for a noticeable higher value of D_{mean}. This result could be expected - the fractal characteristics of the sea surface are widely known in the literature [18], [19] – but should be considered with care, because it involves the estimation of the fractal dimension in an area presenting low signal to thermal noise ratio.

Summarizing, in case of natural surfaces, including the sea surface case, the fractal dimension estimation is independent of the sensor look angle variations and allows distinguishing natural surfaces from sea surface and from urban areas. Conversely, the fractal dimension estimation in case of urban areas is dependent on different sensor look angles and, presently, does not allow a classification between different types of city areas. The fractal dimension maps relevant to natural areas potentially provide a

powerful instrument to the community of SAR end users, and in particular to geologists and geophysicists. The geophysical properties of the imaged surface can be retrieved effectively from their SAR image, and are not dependent on the acquisition geometry in a wide range of practical cases. These maps can be geocoded with standard techniques, providing products which are easily interpreted and managed by non-expert SAR users. As an example, in Fig. 5 3-D visualizations of the fractal dimension maps estimated from the presented set of Cosmo-SkyMed images superimposed to the SRTM DEM of the Vesuvius area are shown, in order to provide a practical demonstration of the versatility of the considered product. This kind of visualization allows appreciating the behavior of the fractal dimension as a function of the height of the surface. For instance, in the case of interest it is interesting to note how the average fractal dimension is the same around the Vesuvius cone, while experiencing a significant change in the Mt. Somma area (on the left in Fig. 5), where the topography of the scene - evaluated at the scales considered for fractal dimension estimation, which are related to the sliding window size - significantly changes [23].

V. Conclusions

In this paper the behavior for changing sensor parameters of an innovative SAR product developed by the authors has been analyzed. The product consists in a fractal dimension map representing the point by point fractal dimension of a surface estimated from a single (amplitude) SAR image. The fractal dimension maps relevant to a data-set of COSMO-SkyMed stripmap images of Naples (Italy), with look angles varying from 22° to 44°, have been considered in the analysis. The considered SAR images are relevant to both an urban area and a natural scenario (the Somma-Vesuvius volcanic complex), thus giving the opportunity to analyze the behavior of the maps for both these situations.

The results of our analysis show that while the fractal dimension estimated from a SAR image relevant to natural areas can be considered to be independent of the look angle and the incidence angle, this does not hold for the fractal dimension pertinent to urban areas where the considered imaging model cannot be assumed and the fractal estimation results depend on the specific SAR acquisition parameters. Moreover, the considered data set is made up of unbalanced, non-calibrated images and, very remarkably, the obtained results showed no dependence on data calibration. The obtained results are of key importance for the applicative community, where the need for products which can be easily managed also by non-expert SAR users is especially strong. In fact, the product we propose can be continuously acquired independently of the acquisition geometry, it can be easily geocoded and projected on Digital Elevation Models, or used in conjunction with other kinds of geo-referenced data.

Finally, due to the clear physical meaning of the estimated parameter, which results to be related only to the roughness of the imaged surface, the realization of a wide set of potential applications can be also considered in the near future. In particular, the fractal dimension maps clearly bear physical information which could be used in support of segmentation and classification of

SAR images. The incidence angle independence could be exploited for the development of new data fusion schemes, based on the invariance of physical characteristics of the scene. Also shape-from-shading algorithms could highly benefit from the peculiarities of the fractal dimension maps demonstrated in the present paper, as mentioned in the Introduction. This list of the possible applications of the presented product is not at all exhaustive and future work is required for a more precise definition of the attainable developments. Definitely, one of the main results of this paper is to clarify that all these new applications can be conceived thanks to the remarkable properties that we demonstrated the fractal dimension map holds.

REFERENCES

[1] M. Datcu, H. Daschiel, A. Pelizzari, M. Quartulli, A. Galoppo, A. Colapicchioni, M. Pastori, K. Seidel, P. G. Marchetti, and S. D'Elia, "Information mining in remote sensing image archives: System concepts", *IEEE Trans. Geosci. Remote Sens.*, vol. 41, no. 12, pp. 2923–2936, Dec. 2003.

[2] B. B. Mandelbrot, *The Fractal Geometry of Nature*. New York: Freeman, 1983.

[3] G. Franceschetti, D. Riccio, *Scattering, Natural Surfaces and Fractals*. Burlington, MA: Academic Press, 2007.

[4] K. Falconer, *Fractal Geometry*. Chichester, U.K.: Wiley, 1989.

[5] J. S. Feder, *Fractals*. New York: Plenum, 1988.

[6] Turcotte D. L., *Fractals and Chaos in Geology and Geophysics*. Cambridge University Press, 1997.

[7] B. A. Campbell, "Scale-dependent surface roughness behavior and its impact on empirical models for radar backscatter", *IEEE Trans. Geosci. Remote Sens.*, vol. 47, no. 10, pp. 3480-3488, Oct. 2009.

[8] W. Dierking, "Quantitative Roughness Characterization of Geological Surfaces and Implications for Radar Signature Analysis," *IEEE Trans. Geosci. Remote Sens.*, vol. 37, no. 5, pp. 2397–2412, Sep. 1999.

[9] M. K. Shepard, B. A. Campbell, M. H. Bulmer, T. G. Farr, L. R. Gaddis, and J. J. Plaut, "The roughness of natural terrain: A planetary and remote sensing perspective", *J. Geophys. Res.*, vol. 106, no. E12, pp. 32 777–32 795, Dec. 2001.

[10] S. R. Brown and C. H. Scholz, "Broad-band study of the topography of natural rock surfaces," *J. Geophys. Res.*, vol. 90, no. B14, pp. 12 575–12 582, Dec. 1985.

[11] L. R. Gaddis, P.J. Mouginis-Mark, and J.N. Hayashi, "Lava flow surface textures: SIR-B radar image texture, field observations, and terrain measurements", *Photogrammetric Eng. Remote Sens.*, vol. 56, pp. 211-224, Feb. 1990.

[12] B. A. Campbell and M. K. Shepard, "Lava flow surface roughness and depolarized radar scattering," *J. Geophys. Res.*, vol. 101, no. E8, pp. 18 941– 18 952, Aug. 1996.

[13] T. Austin, A. W. England, G. H. Wakefield, "Special problems in the estimation of power-law spectra as applied to topographical modeling", *IEEE Trans. Geosci. Remote Sens.*, vol. 32, no. 4, pp. 928-939, July 1994.

[14] G. Franceschetti, P. S. Callahan, A. Iodice, D. Riccio, and S. D. Wall, "Titan, Fractals, and Filtering of Cassini Altimeter Data," *IEEE Trans. Geosci. Remote Sens.*, vol. 44, no. 8, pp. 2055–2062, Aug. 2006.

[15] A. Heck and J. M. Perdang, *Applying Fractals in Astronomy*. Lecture Notes in Physics Vol. m3, Berlin: Springer, 1991.

[16] B. Pesquet-Popescu, J. L. Véhel, "Stochastic fractal models for image processing," *IEEE Signal Processing Magazine*, vol. 19, no. 5, pp. 48- 62, Sep. 2002.

[17] J. L. Véhel and E. Lutton, *Fractals in Engineering*. New York, NJ: Springer Verlag, 2005.

[18] R. E. Glazman, "Fractal Nature of Surface Geometry in a Fractal Sea", in *Non-linear Variability in Geophysics: Scaling and Fractals*, Dordrecht: Kluwer Academic Publishers, 1991.

[19] Ulaby, F. T., R. K. Moore, and A. K. Fung, *Microwave Remote Sensing*, Addison-Wesley, 1981.

[20] G. Di Martino, A. Iodice, D. Riccio, and G. Ruello, "Imaging of Fractal Profiles", *IEEE Trans. Geosci. Remote Sens.*, vol. 48, no. 8, pp. 3280-3289, Aug. 2010.

[21] G. Di Martino, D. Riccio, and I. Zinno, "SAR Imaging of Fractal Surfaces", *IEEE Trans. Geosci. Remote Sens.*, vol. 50, no. 2, pp. 630-644, Feb. 2012.

[22] G. Di Martino, A. Iodice, D. Riccio, G. Ruello, and I. Zinno, "Fractal Based Filtering of SAR Images", *Proceedings IGARSS 2010*, pp. 2984-2987, July 2010.

[23] G. Di Martino, A. Iodice, D. Riccio, G. Ruello, and I. Zinno, "On the fractal nature of volcano morphology detected via SAR image analysis: the case of Somma–Vesuvius Volcanic Complex", *European Journal of Remote Sensing*, no. 45, pp. 177-187, 2012.

[24] G. Di Martino, G. Franceschetti, D. Riccio, and I. Zinno, "Spectral processing for the extraction of fractal parameters from SAR data", *Proceedings of DSP 2011*, pp. 1-7, July 2011.

[25] W.T. Crow, W. Wagner, and V. Naeimi, "The Impact of Radar Incidence Angle on Soil-Moisture-Retrieval Skill," *IEEE Geosci. Remote Sens. Lett.*, vol. 7, no. 3, pp. 501-505, July 2010.

[26] A. P. Pentland, "Local Shading Analysis", *IEEE Trans. Pattern Anal. and Machine Intell.*, vol. PAMI-6, no. 2, pp. 170-187, March 1984.

[27] A. P. Pentland, "Linear shape from shading", *Int. J. Computer Vision*, vol. 1, no. 4, pp. 153-162, 1990.

[28] B. Waske and J. A. Benediktsson, “Fusion of support vector machines for classification of multisensor data”, *IEEE Trans. Geosci. Remote Sens.*, vol. 45, no. 12, pp. 3858–3866, Dec. 2007.

[29] G. Di Martino, A. Iodice, D. Riccio, G. Ruello, and I. Zinno, “Fractal Filtering Applied to SAR Images of Urban Areas”, *Proceedings of JURSE 2011*, pp. 261-264, April 2011.

[30] J. Capon, “High-Resolution Frequency-Wavenumber Spectrum Analysis,” *Proceedings of the IEEE*, vol. 57, no. 8, pp. 1408–1418, Aug. 1969.

[31] S. M. Kay, *Modern Spectral Analysis*. Englewood Cliffs, NJ: Patience Hall, 1999.

[32] A. Freeman, “SAR calibration: An overview”, *IEEE Trans. Geosci. Remote Sens.*, vol. 30, no. 6, pp. 1107–1121, Nov. 1992.

[33] J. J. van Zyl, B. D. Chapman, P. Dubois, and J. Shi, “The effect of topography on SAR calibration”, *IEEE Trans. Geosci. Remote Sens.*, vol. 31, no. 5, pp. 1036–1043, Sep. 1993.

[34] S. Gernhardt, X. Cong, M. Eineder, S. Hinz, R. Bamler, "Geometrical Fusion of Multitrack PS Point Clo*uds", IEEE Geosci. Remote Sens. Lett.*, vol. 9, no. 1, pp. 38-42, Jan. 2012.

[35] M. Karjalainen, "Geocoding of Synthetic Aperture Radar Images Using Digital Vector Maps", *IEEE Geosci. Remote Sens. Lett.*, vol. 4, no. 4, pp. 616-620, Oct. 2007.

Figure captions

Fig. 1 Theoretical log-log plots of range (continuous line) and azimuth (dash-dot line) image cuts PSD; the dashed line represents the surface cut PSD.

Fig. 2 Regions of interest of the considered Cosmo-SkyMed data set (on the left) and relevant fractal dimension maps (on the right). From (a) to (c) the images are relevant to the Vesuvius area acquired with different look angles: (a) 22°, (b) 31°, and (c) 44°. From (d) to (f) the images are relevant to the Naples urban area acquired with the same look angles: (d) 22°, (e) 31°, and (f) 44°.

Fig. 3 Geocoded version of the fractal dimension maps presented in Fig. 1. From (a) to (c) the images are relevant to the Vesuvius area: (a) 22°, (b) 31°, and (c) 44°. From (d) to (f) the images are relevant to the Naples urban area: (d) 22°, (e) 31°, and (f) 44°. The selected test sites are marked in red.

Fig. 4 Histograms for different look angles of the eight test sites: from (a) to (d) they are relevant to the Vesuvius area, while from (e) to (h) they are relevant to the urban area, according to what reported in Tab. I and II. In each plot the histograms relevant to different look angles are compared: 22° solid line, 31° dashed line, 44° dash-dot line. The 200x200 pixels areas relevant to the different look angles are reported under each histogram.

Fig. 5 3-D view of the fractal dimension maps of the Vesuvius area estimated from the three SAR images: (a) 22°, (b) 31° and (c) 44°.

Figures and Tables

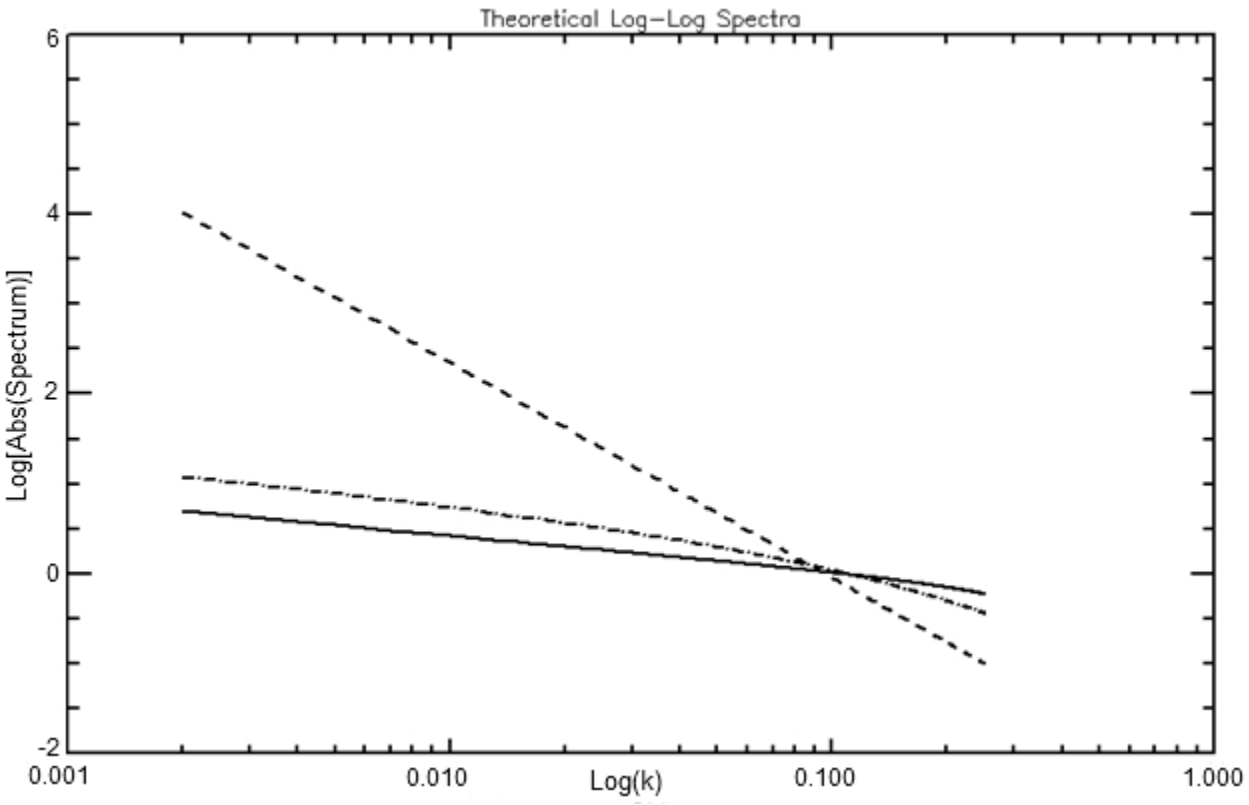

Fig. 1

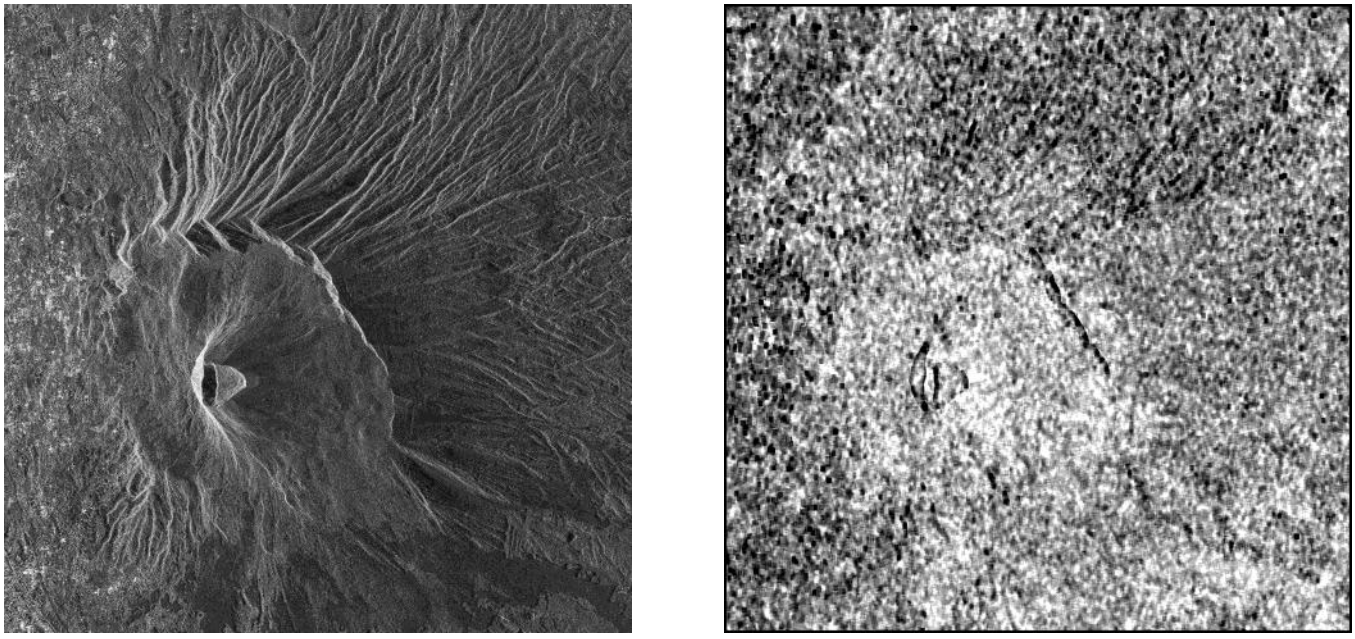

(a)

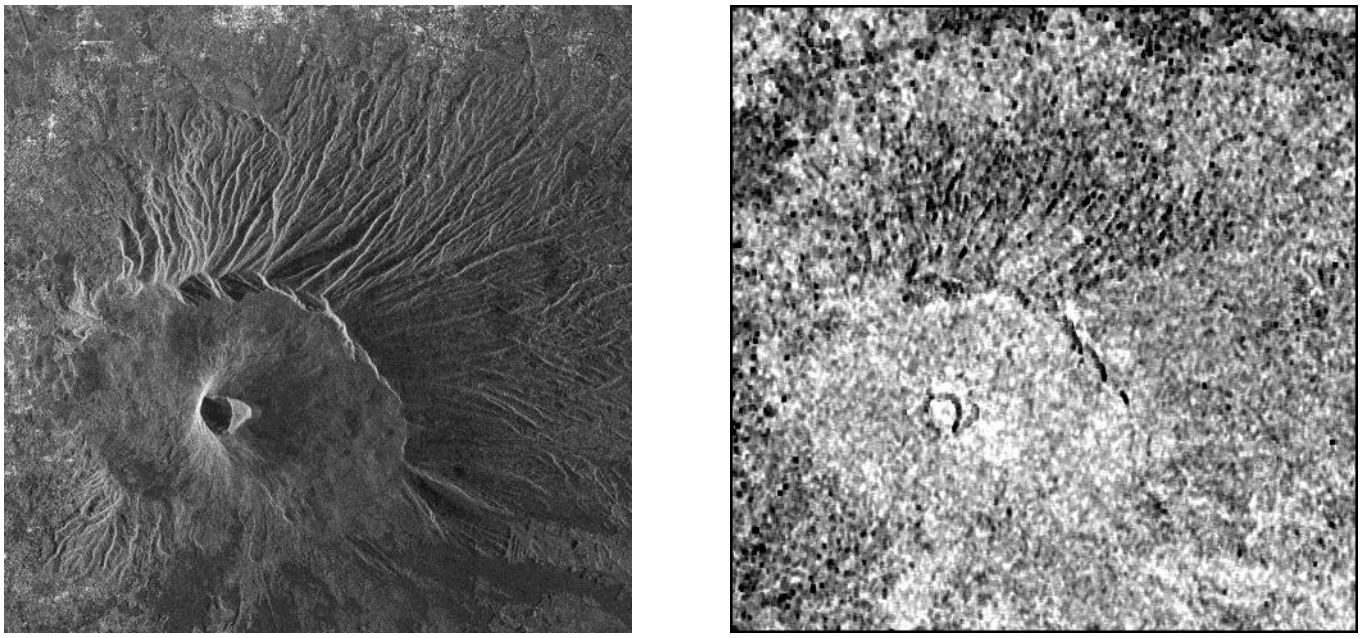

(b)

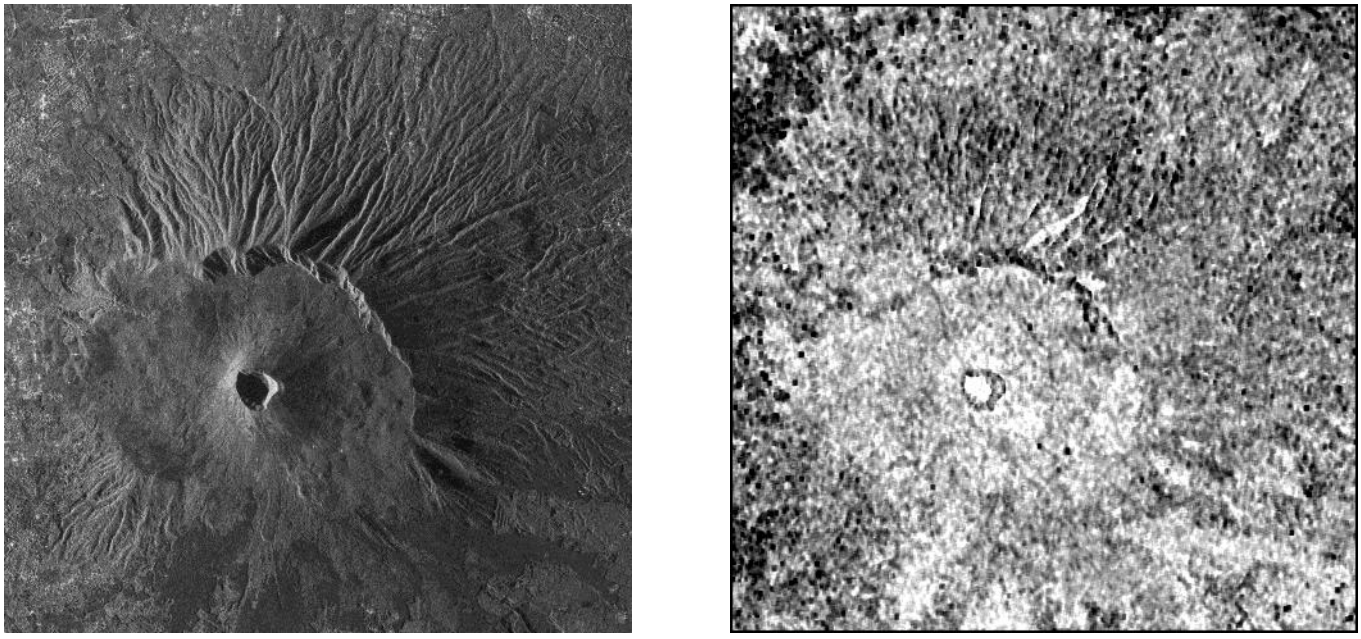

(c)

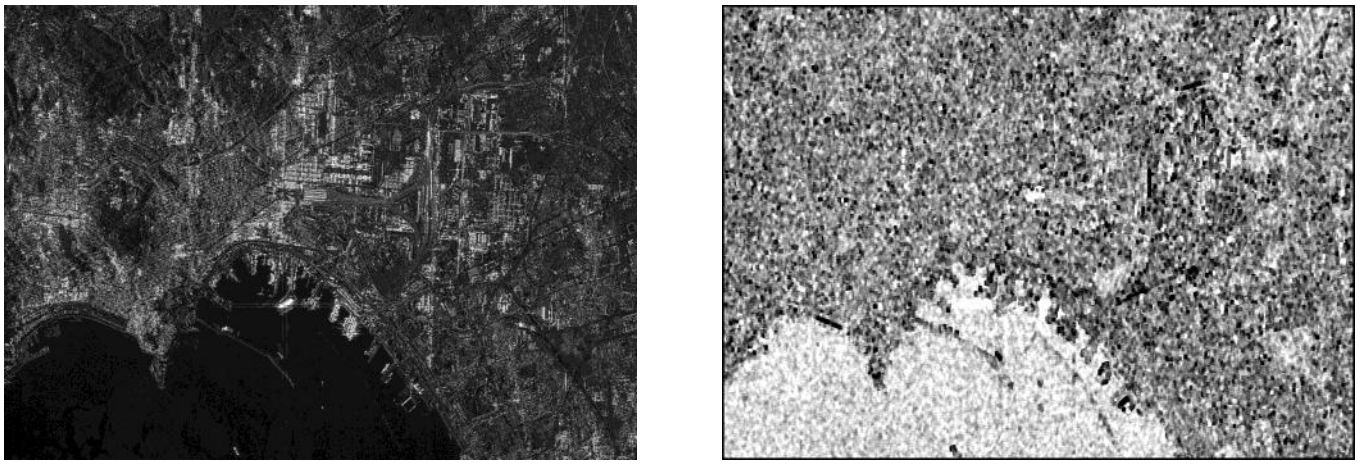

(d)

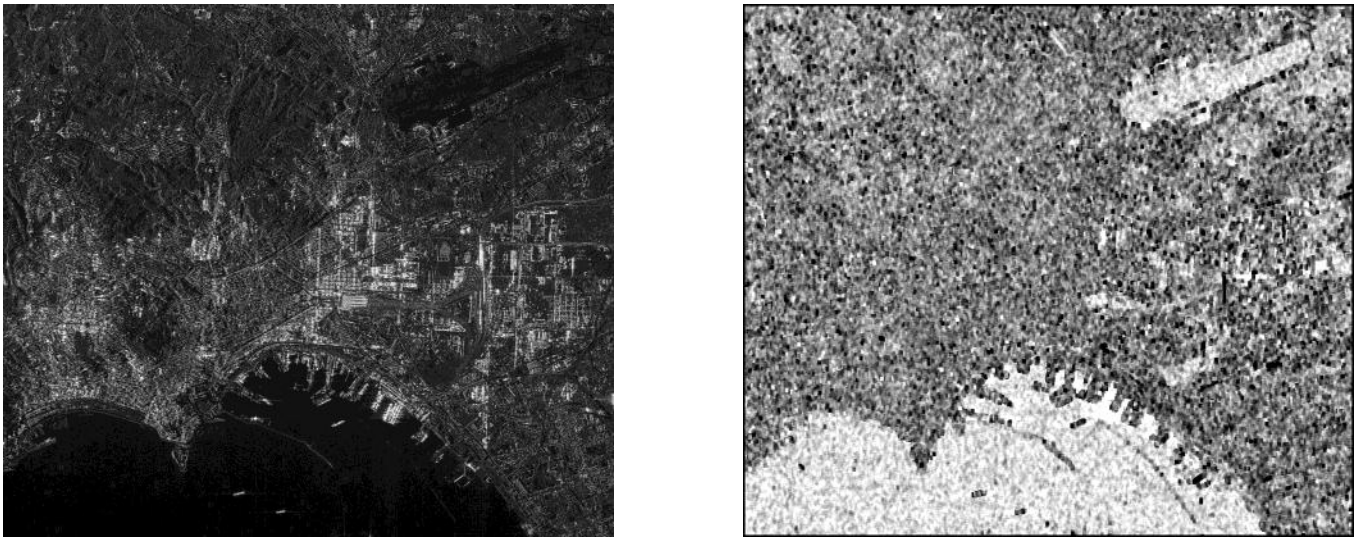

(e)

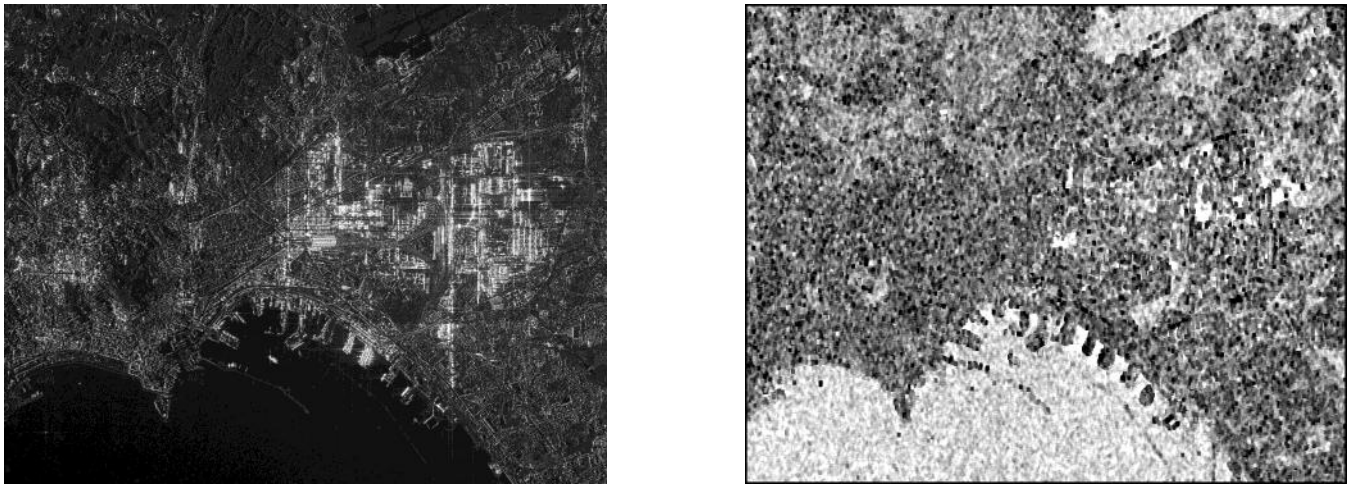

(f)

Fig. 2

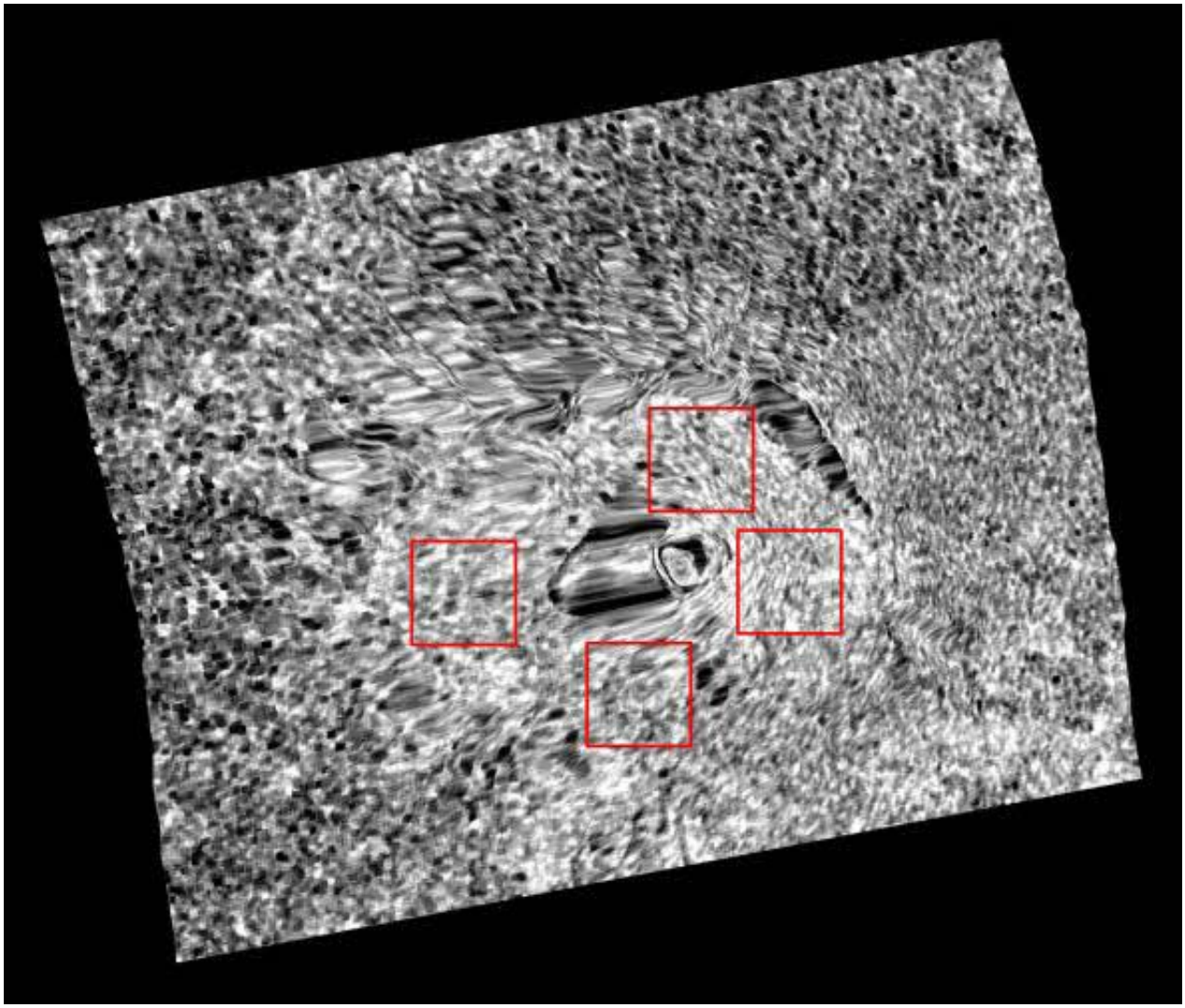

(a)

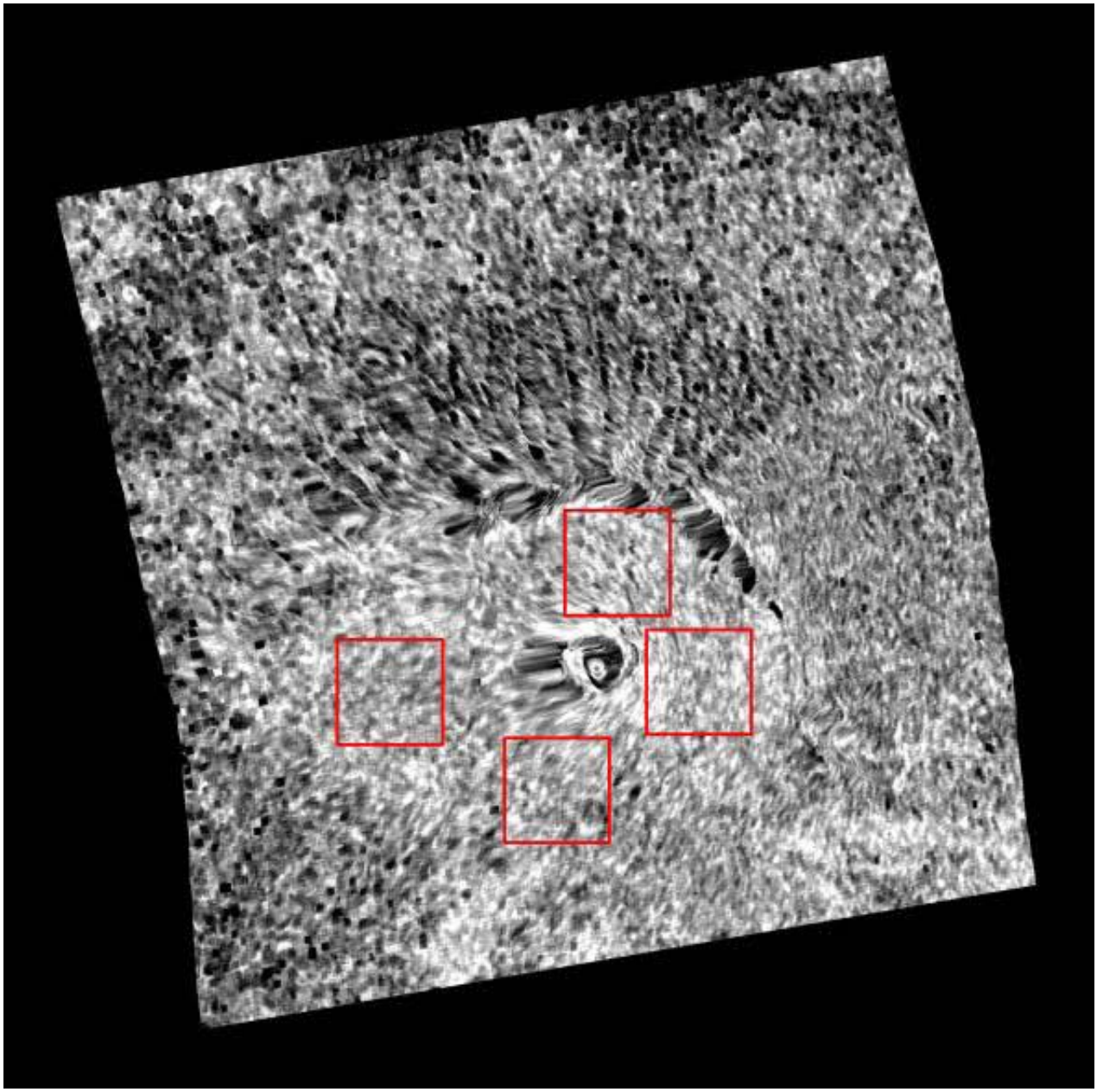

(b)

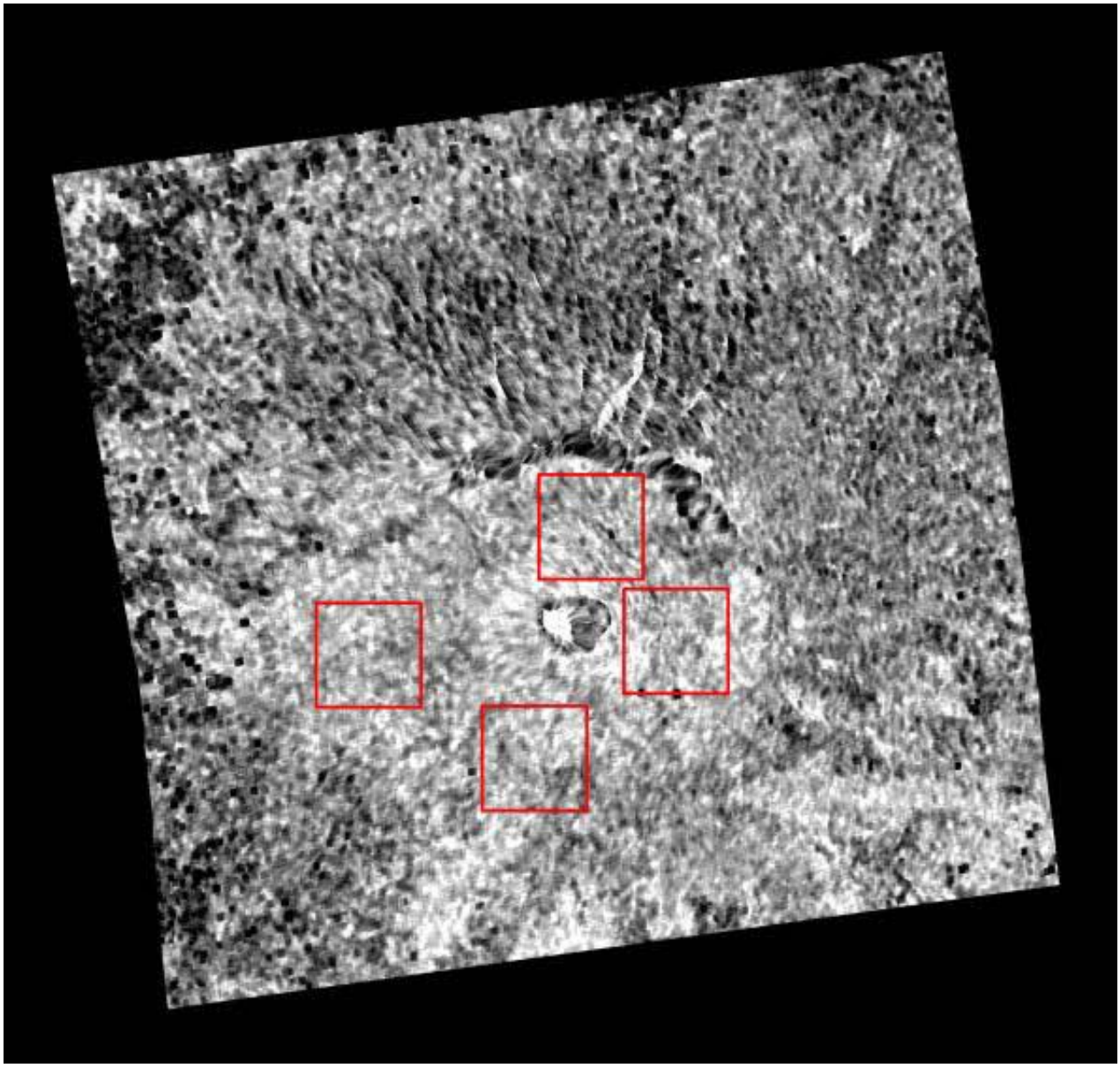

(c)

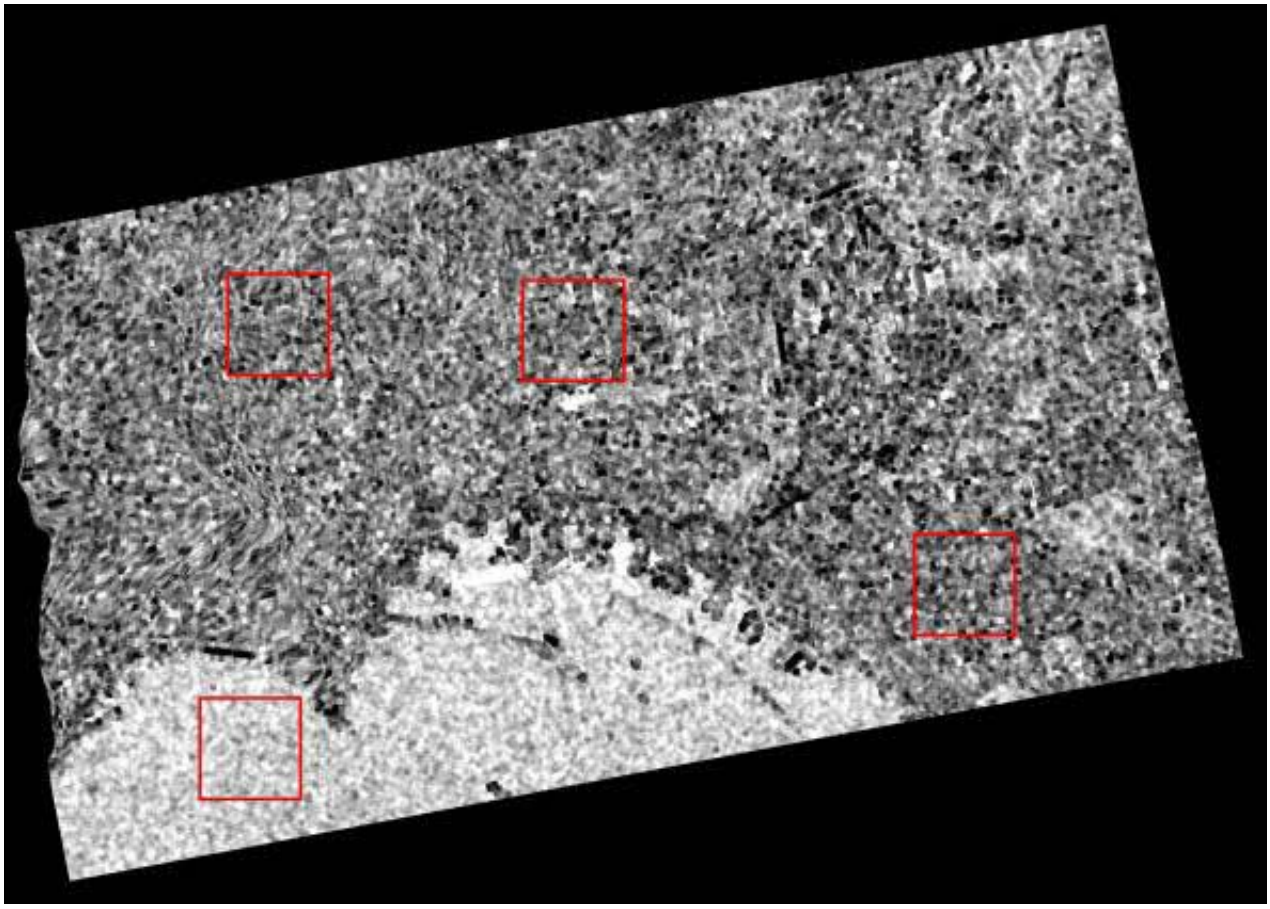

(d)

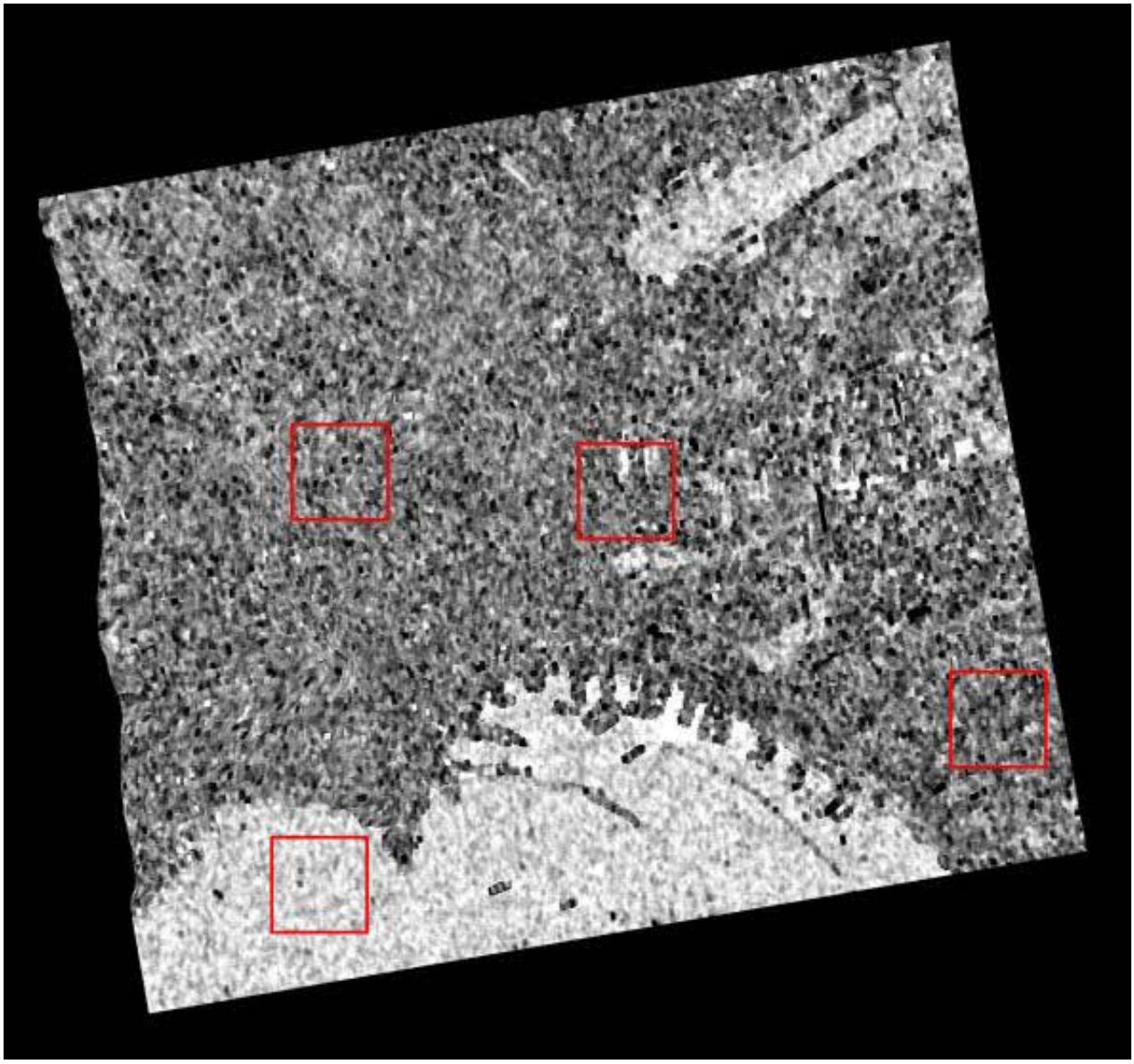

(e)

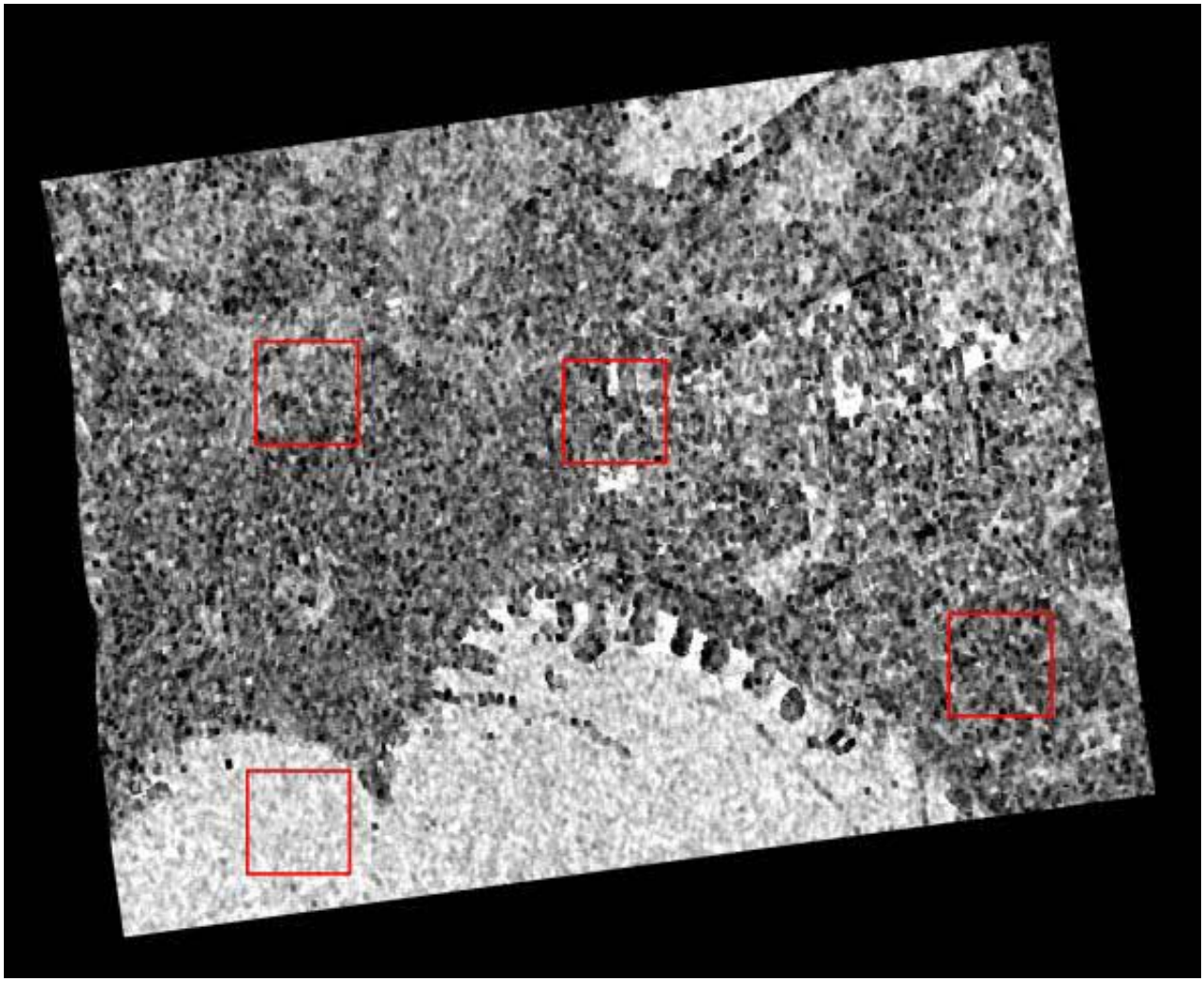

(f)

Fig. 3

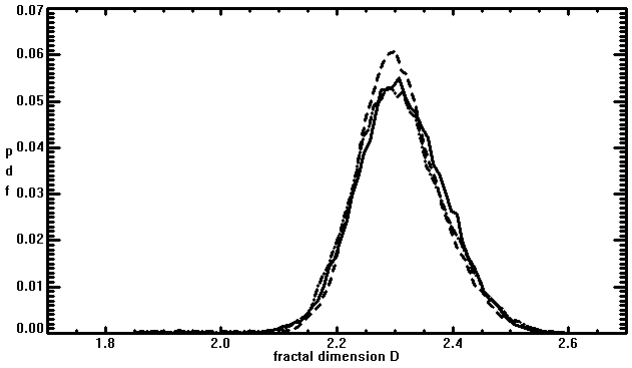

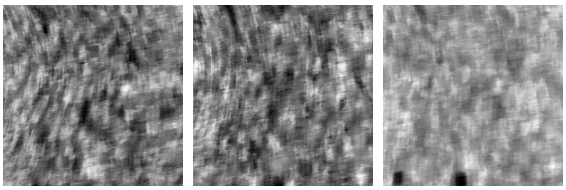

22° 31° 44°

(a)

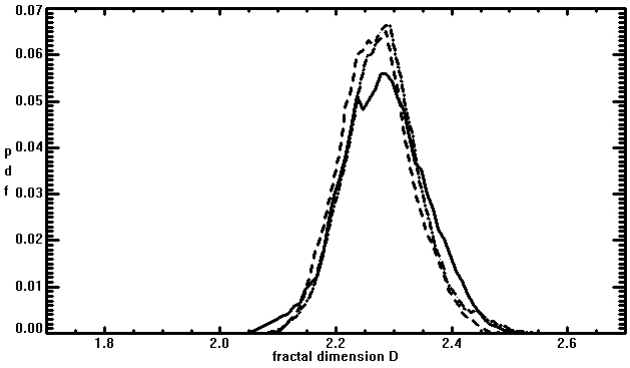

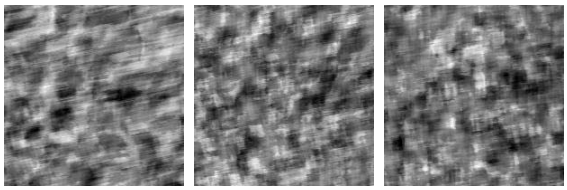

22° 31° 44°

(b)

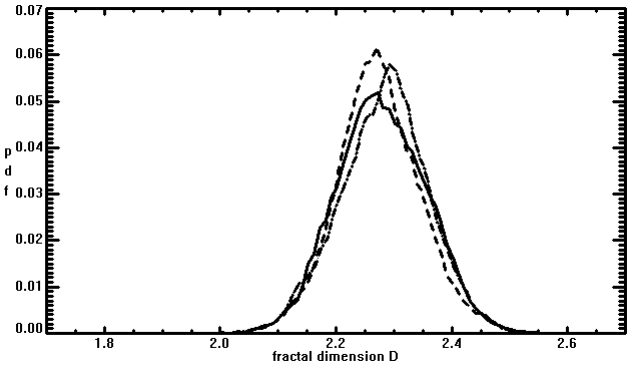

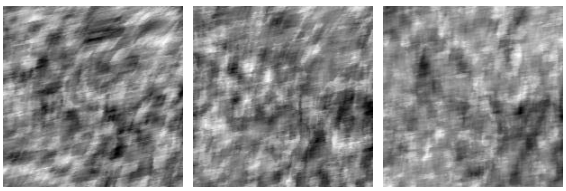

22° 31° 44°

(c)

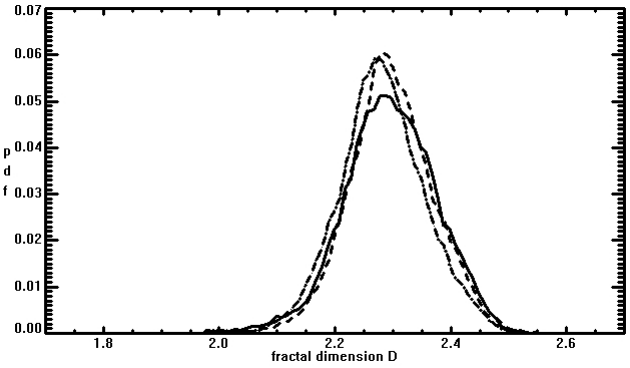

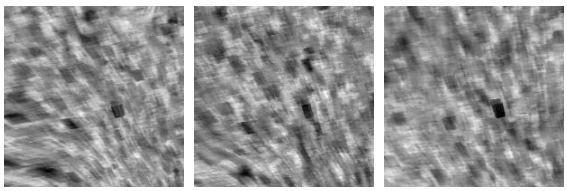

22° 31° 44°

(d)

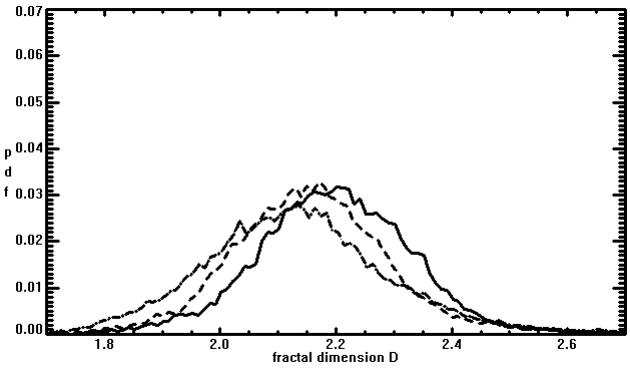

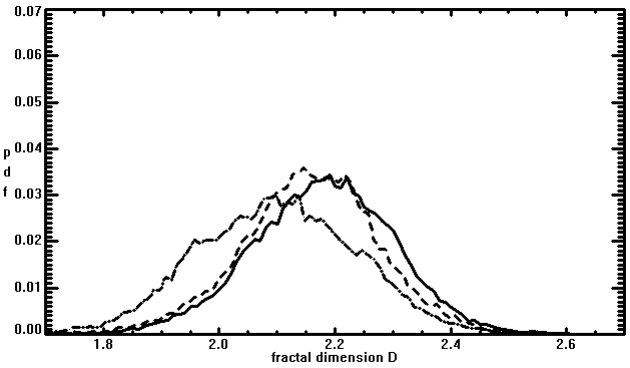

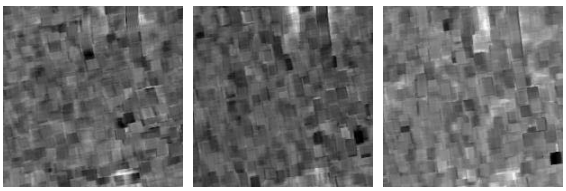

22° 31° 44°

(e)

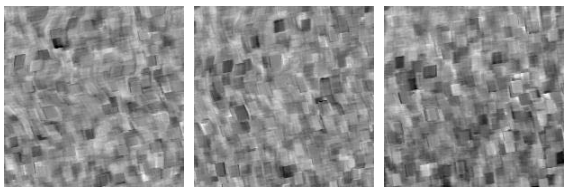

22° 31° 44°

(f)

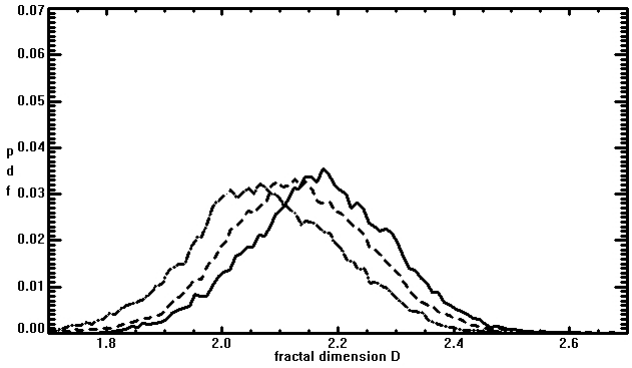

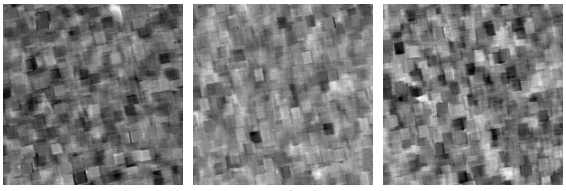

22° 31° 44°

(g)

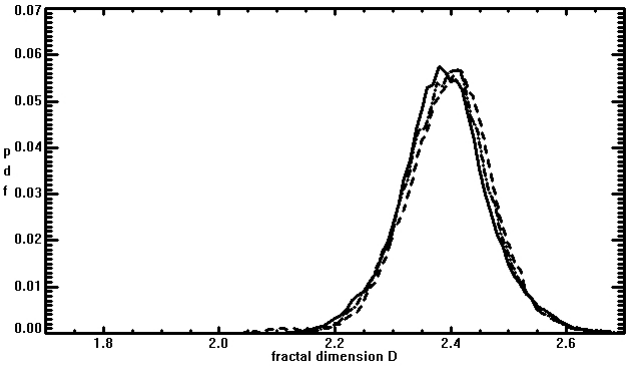

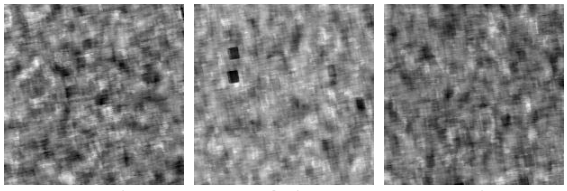

22° 31° 44°

(h)

Fig. 4

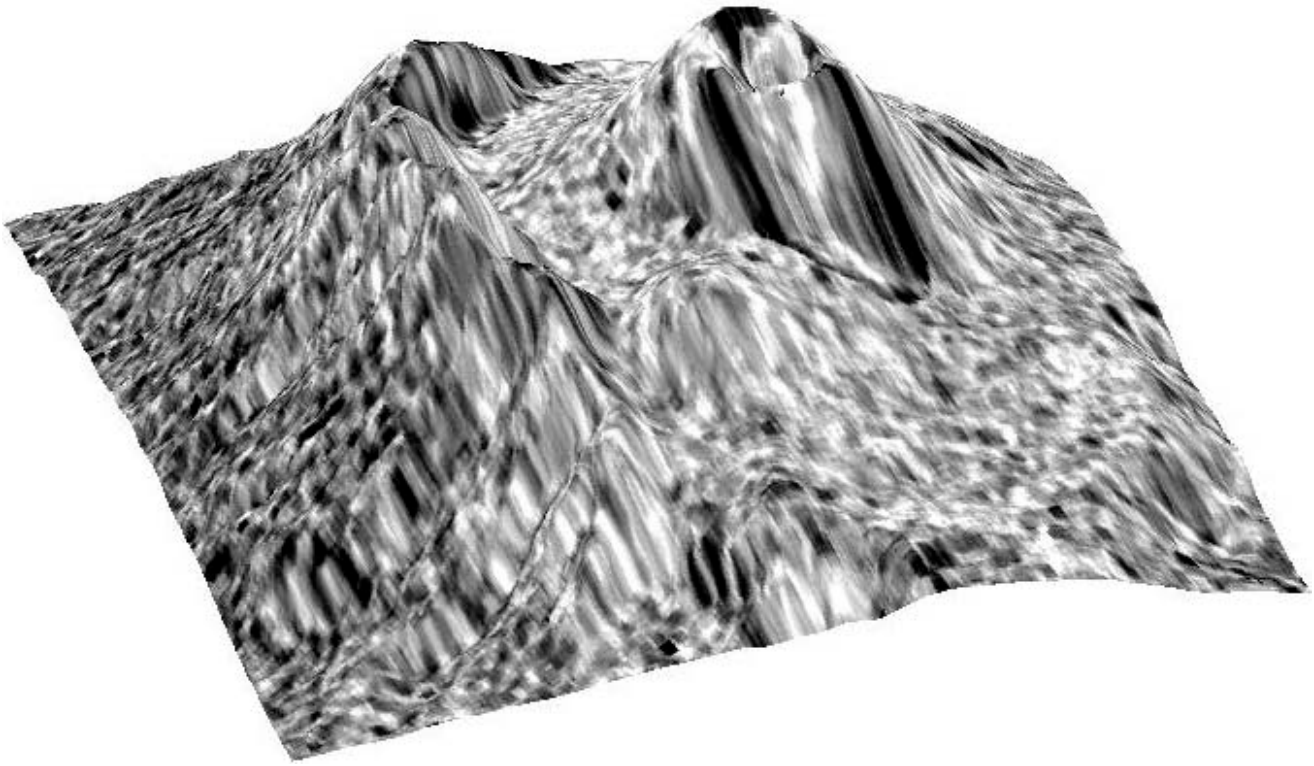

(a)

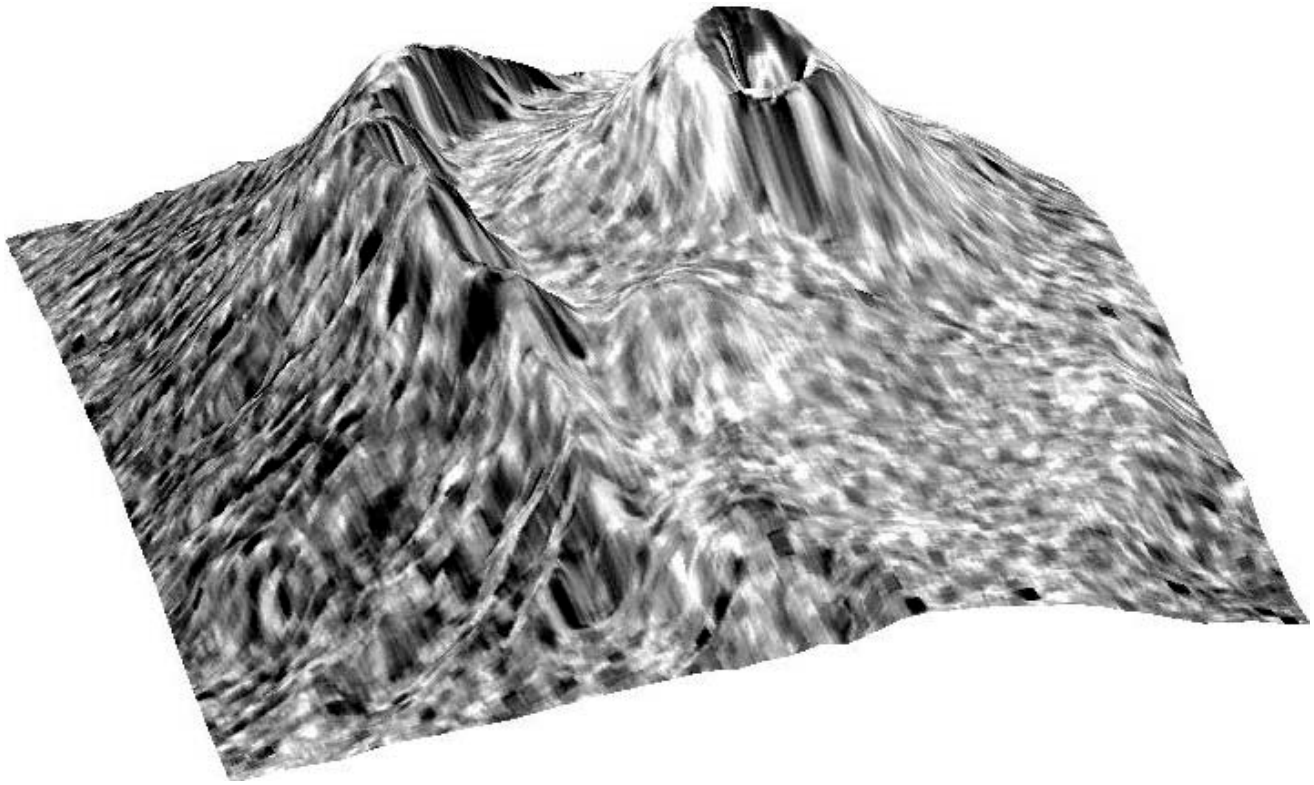

(b)

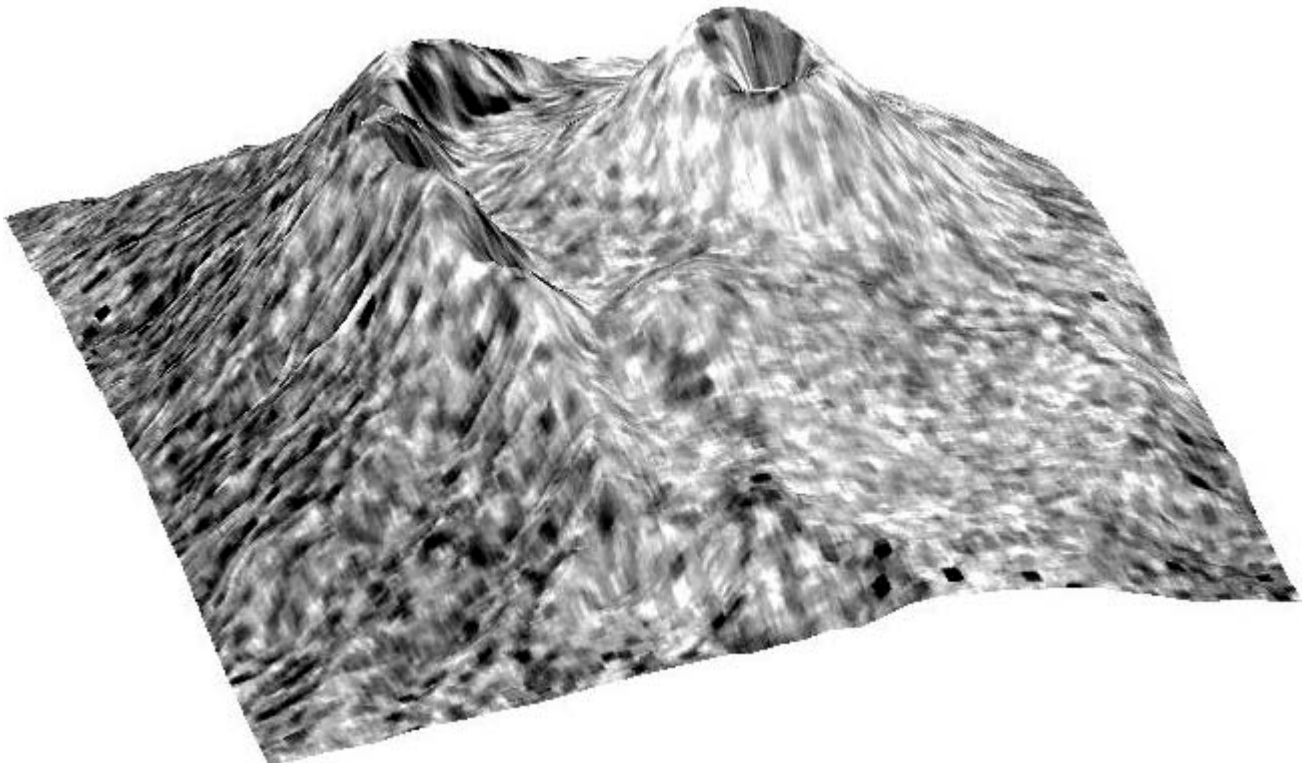

(c)

Fig. 5

TABLE I
STATISTICS OF THE VESUVIUS SUBSETS

Subset	θ_0	$D_{1\%}$	$D_{99\%}$	D_{mean}	D_{stdev}
Back-slope Fig. 3 (a)	22°	2.14	2.49	2.32	0.07
	31°	2.17	2.50	2.31	0.07
	44°	2.11	2.50	2.31	0.08
Fore-slope Fig. 3 (b)	22°	2.12	2.46	2.29	0.07
	31°	2.14	2.43	2.27	0.06
	44°	2.14	2.47	2.29	0.06
Forward Fig. 3 (c)	22°	2.11	2.46	2.28	0.08
	31°	2.12	2.47	2.28	0.07
	44°	2.11	2.46	2.29	0.08
Backward Fig. 3 (d)	22°	2.10	2.48	2.30	0.08
	31°	2.13	2.48	2.30	0.07
	44°	2.11	2.47	2.29	0.07

TABLE II
STATISTICS OF THE URBAN SUBSETS

Subset	θ_0	$D_{1\%}$	$D_{99\%}$	D_{mean}	D_{stdev}
Business Fig. 3 (e)	22°	1.86	2.59	2.20	0.14
	31°	1.82	2.68	2.17	0.16
	44°	1.75	2.72	2.14	0.18
Semi-urban Fig. 3 (f)	22°	1.88	2.47	2.18	0.12
	31°	1.85	2.44	2.16	0.12
	44°	1.78	2.43	2.10	0.14
Historical Fig. 3 (g)	22°	1.89	2.48	2.18	0.13
	31°	1.82	2.44	2.13	0.13
	44°	1.77	2.37	2.08	0.13
Sea Fig. 3 (h)	22°	2.21	2.59	2.39	0.08
	31°	2.18	2.59	2.40	0.08
	44°	2.22	2.60	2.40	0.08